NASA Contractor Report 182281

Finite Element Modeling of Frictionally Restrained Composite Interfaces

Roberto Ballarini and Shamim Ahmed
Case Western Reserve University
Cleveland, Ohio

April 1989

Prepared for
Lewis Research Center
Under Grant NAG3-856

National Aeronautics and
Space Administration

FINITE ELEMENT MODELING OF FRICTIONALLY RESTRAINED COMPOSITE INTERFACES

Roberto Ballarini and Shamim Ahmed
Department of Civil Engineering
Case Western Reserve University
Cleveland, OH 44106

SUMMARY

This paper describes the use of special interface finite elements to model frictional restraint in composite interfaces. These elements simulate Coulomb friction at the interface, and are incorporated into a standard finite element analysis of a two-dimensional isolated fiber pullout test. Various interfacial characteristics, such as the distribution of stresses at the interface, the extent of slip and delamination, load diffusion from fiber to matrix, and the amount of fiber extraction or depression are studied for different friction coefficients. The results are compared to those obtained analytically using a singular integral equation approach , and those obtained by assuming a constant interface shear strength. The usefulness of these elements in micromechanical modeling of fiber-reinforced composite materials is highlighted.

INTRODUCTION

In composite materials with brittle constituents, such as ceramic matrix composites, the fiber and matrix are unbonded, and are restrained by frictional forces at the interface. In such composites, the interface has been modeled [1,2,3] as having a constant interface shear strength τ_0, and for shear stresses greater than τ_0, slipping occurs at the interface. This means of analyzing load transfer is approximate, and it is not clear for which conditions it is appropriate.

A more realistic analysis of interfacial load transfer, described by Coulomb friction, has been recently presented by Dollar and Steif [4]. Instead of assuming a constant interface shear strength beyond which slip occurs, the maximum stress that the interface can sustain is related to the prevailing normal

stress, σ_n, and the coefficient of friction at the interface, μ, by the relation

$$\tau_0 = \mu \, |\sigma_n| \tag{1}$$

Thus the allowable shear stress changes with the level of the applied load, and with the depth of the fiber.

According to this friction law, at any instant in the loading history, either sticking, slipping or opening occurs at a generic point along the interface. Conditions for these three states are as follows:

(a) Stick: $\sigma_n < 0$ (compressive)

$$|\tau| \leq \mu |\sigma_n|,$$

$$dg/dt = 0, \text{ and}$$

$$h = dh/dt = 0 \tag{2}$$

(b) Slip : $\sigma_n < 0$

$$|\tau| = \mu |\sigma_n| ,$$

$$\text{sgn}(dg/dt) = \text{sgn}(\tau),$$

$$h = dh/dt = 0 \tag{3}$$

(c) Open (equivalent to interface cracking):

$$\sigma_n = 0,$$

$$\tau = 0, \text{ and}$$

$$h > 0 \tag{4}$$

In these equations, g and h represent the relative slip and separation between the fiber and the matrix respectively, while d()/dt is the derivative with respect to a time-like parameter that increases monotonically as the loading proceeds.

The above analysis was used to study the load transfer and slip lengths for the simple problem of a two-dimensional fiber pullout (and indentation) test (Fig. 1). An analytical integral equation approach was used to obtain the solution for the half plane problem with the fiber loaded with an axial stress p (tension or compression), and subjected to a uniform lateral compressive prestress, σ_0. Their results indicate that the extent of slipping as well as the rate of load transfer from the fiber to the matrix may be significantly different from those predicted by using the constant shear stress approximation, particularly for high compressive stresses, p. In order to avoid added mathematical

complexity, the authors have not incorporated the opening case in their analysis, and have also assumed that both the fiber and the surrounding matrix are made of the same material.

This paper describes the use of special interface friction elements in a finite element model of the problem described. These special elements employ incremental elasto-plastic constitutive relationships to simulate realistic frictional restraint at composite interfaces. This model is capable of implementing all the interface conditions mentioned earlier and can also be extended to consider non-homogeneous interfaces and more complicated finite geometries.

DESCRIPTION OF THE FRICTION ELEMENT

A two-dimensional quadratic displacement finite element for contact friction problems was developed by Ballarini, Parulekar and Plesha [5] for modeling rough, dilatant rock joints, and has proved to be quite useful for handling such elastic-plastic friction problems. A brief description of the friction model will be given here. Each friction element shown in Fig. 2 has zero thickness, and 6 nodes with two degrees of freedom at each node corresponding to displacements u_t and u_n, tangential and normal to the plane of the surface respectively. The constitutive law we adopt in this paper was fully developed by Plesha [6], and is analogous to the theory of continuum elasto-plasticity.

The kinematic variables used in the constitutive law are the relative surface displacements in the tangential and normal directions, which are defined as

$$g_t = (\vec{u}_B - \vec{u}_A)\cdot \vec{t}$$
$$g_n = (\vec{u}_B - \vec{u}_A)\cdot \vec{n}\ , \qquad (5)$$

where $\vec{u}_A$ and $\vec{u}_B$ are the displacement vectors of adjacent points on the interface associated with the two phases A and B respectively, and $\vec{t}$ and $\vec{n}$ are unit vectors in the tangent and normal directions of the interface respectively. The tangential and normal stresses the interface supports at any point are denoted by σ_t and σ_n respectively, with the convention that compressive stresses are negative.

A basic assumption in the theory is that the deformation can be additively decomposed into

$$g = g_i^e + g_i^p \qquad i = t,\ n \qquad (6)$$

where superscripts e and p denote elastic (recoverable) and plastic (irrecoverable) parts of the deformation and subscript i denotes a vector component in the tangent or normal direction. This provides the advantage of leading to a more convenient numerical implementation compared to frictional idealizations adopted in this paper in which a "stick" condition precedes frictional sliding.

The elastic displacements are related to stresses by the elastic constitutive law $d\sigma_{ij} = E_{ij} dg_i^e$, while plastic deformations obey the following slip rule

$$dg_i^p = \begin{cases} 0 \text{ if } F < 0 \text{ or } dF < 0 \text{ (no slip)} \\ \lambda \dfrac{\partial G}{\partial \sigma_i} \text{ if } F = dF = 0 \text{ (slip)} \end{cases} \tag{7}$$

where E_{ij} are the interface stiffnesses (E_{nn}, E_{nt}, E_{tt}, E_{tn}) that have units of force per unit volume,

g_i is the sum of the elastic (pre-slip) and plastic (post-slip) displacements at any load level,

F is a slip function given by $F = |\sigma_t| + \mu\sigma_n$,

G is a slip potential given by $G = |\sigma_t|$, and

λ is a non-negative scalar which gives the magnitude of slip.

For elasto-plastic analysis, the element employs an incremental constitutive law relating increments of stress to increments of total relative displacements:

$$d\sigma_i = E_{ij} \left\{ g_j - \frac{\dfrac{\partial F}{\partial \sigma_p} E_{pq} \, dg_q}{\dfrac{\partial F}{\partial \sigma_p} E_{pq} \dfrac{\partial G}{\partial \sigma_q}} \frac{\partial G}{\partial \sigma_j} \right\} \tag{8}$$

Since the above explicit relationship is incremental, it is valid for arbitrary load and deformation histories that can involve loading and subsequent unloading (changes in the direction of frictional sliding, for example).

It has been shown [6] that $E_{nt} = E_{tn} = 0$, hence, for no-slip, Eq. (8) reduces to

$d\sigma_t = E_{tt} dg_t$, and

$d\sigma_n = E_{nn} dg_n$, or in the matrix form,

$$\begin{bmatrix} d\sigma_t \\ d\sigma_n \end{bmatrix} = \begin{bmatrix} E_{tt} & 0 \\ 0 & E_{nn} \end{bmatrix} \begin{bmatrix} dg_t \\ dg_n \end{bmatrix}, \tag{9}$$

while for the slip case, Eq. (8) becomes

$d\sigma_t = -\mu E_{nn} \, sgn(\sigma_t) dg_n$, and

$d\sigma_n = E_{nn} \, dg_n$, or,

$$\begin{bmatrix} d\sigma_t \\ d\sigma_n \end{bmatrix} = \begin{bmatrix} 0 & -\mu E_{nn} sgn(\sigma_t) \\ 0 & E_{nn} \end{bmatrix} \begin{bmatrix} dg_t \\ dg_n \end{bmatrix} \tag{10}$$

When the fiber and matrix separate under normal tensile stress, the interface carries no further stress, Eq. (4). Hence for the opening condition, the stiffness of the interface element is set to zero.

Mathematically, E_{nn} and E_{tt} are penalty numbers, and in order to satisfy Eqs. (2)-(4), their values must be manipulated so as to obtain the type of rigid-perfectly plastic response shown in Fig. 3. Eq. (4) allows no normal separation at the interface until the normal stress, σ_n, turns tensile. Hence E_{nn} should be as high as possible for $\sigma_n < 0$ (compressive), but at the same time should not create numerical problems in the solution procedure. Similarly, Eq. (2) requires that the elastic part of the tangential displacement (g in the pre-slip condition) be invariant with respect to the load steps. A parametric study was therefore conducted to determine the appropriate stiffness coefficients which abide by Eqs. (2) to (4). The following sections present the finite element analysis and discussion of the results.

THE ANALYSIS

The finite-element model of the half plane fiber pullout (or indentation) setup is shown in Fig. 4 (not to scale). Symmetry was used to discretize only one half of the domain into 192, 8-node isoparametric rectangular elements, while the special zero-thickness friction elements were employed at the interface. The fiber elements are bound to those of the surrounding matrix

through the enforcement of displacement compatibility with the interface elements.

A transient finite element analysis employing an explicit time integration scheme developed in Ballarini et. al. [5] is implemented in this problem. The load is applied on the fiber in small increments, and convergence is observed for step sizes greater than 50. The average tangential and normal stresses are calculated in each interface element for each load step, and Eqs. (2) to (4) are used for determining the stiffness of the interface elements at the next load step.

RESULTS AND DISCUSSION

In order to check the results of the finite element model, various interfacial characteristics, such as the distribution of interfacial stresses, the extent of slip and opening, load diffusion in the fiber, and slip at the surface are studied for various constitutive properties and are compared to those obtained by Dollar and Steif [4].

Parametric Studies for E_{nn} and E_{tt}.

The Young's modulus, E, for the fiber and matrix is assumed as 400 GPa. Different values of E_{nn} and E_{tt} were used to study the behavior of the interface elements with respect to conformity with Eqs. (2) to (4). It was observed that in order to satisfy Eqs.(2) to (4), the E_{nn} required is as high as 1.0E15 N/m^3, while E_{tt} has to be higher than 1.0E14 N/m^3.

Interfacial Stresses Under Perfectly Bonded Conditions.

Perfect bonding between the fiber and matrix is obtained by removing the friction elements from the interface. The interfacial stress distributions under such conditions was studied in order to check the validity of the finite element model, since exact solutions for various stresses at the perfectly bonded interface are available in the literature.

The distribution of shear and normal tractions, τ and σ_n respectively, due to axial tensile loading of the perfectly bonded half-plane with respect to the depth of the fiber is shown in Fig. 5 for σ_0=0. These are in excellent agreement with analytical solutions for τ and σ_n [4] given by

$$\tau(d) = \frac{-4p}{\pi(d^2+4)}, \quad \sigma_n(d) = \frac{p}{\pi}\left[\frac{\pi}{2} - \tan^{-1}(d/2) - \frac{2d}{d^2+4}\right] \qquad (11)$$

where d=depth into the fiber/fiber radius

$= -y/a$

Variation of Slip Lengths, l_s and delamination lengths, l_0.

When the fiber is loaded in tension, the shear stress τ is maximum at the loading surface (y=0). Slipping takes place when the interfacial shear stress τ is greater than the allowable shear stress $\tau_0 = \mu|\sigma_n|$. The variation of the extent of slip, l_s, with load for different friction coefficients, μ, is plotted in Fig. 6. The extent of slip increases with load and diminishing friction coefficient, since τ_0 is correspondingly smaller. These curves are abruptly ended at points where the interface normal stress turns tensile, and hence separation occurs at the interface. Fig. 7 shows the extent of the delamination lengths, l_0 for various μ. The depth of interfacial opening increases with the tensile load and diminishing μ.

When the fiber is loaded in compression (indentation), slip first initiates at a depth from the surface ranging from one to three fiber radii (Fig. 6), and spreads both in depth and towards the surface with increasing load. For similar loads, l_s for compression is less than that for applied tension, particularly for high μ, where slips initiates at much higher applied loads. No opening was observed to occur under compressive loads. The results compare very well with those presented in Dollar et. al. [4] (they are not duplicated on these plots for the sake of clarity).

Load Transfer from Fiber to Matrix.

Stresses are transferred from the fiber to the matrix (or vice versa) through the interfacial shear stresses. The variation of the axial tensile (and compressive) stresses carried by the fiber, σ_f, with respect to the fiber depth is shown in Fig. 8. For purposes of comparison with the results in Dollar et. al. [4]. the applied load was fixed at $|p/\mu\sigma_0| = \pm 10$, and again, the agreement was found to be very good. It is observed that the load diffusion is faster for compression than for tension. This is due the fact that for compressive loadings, the interface normal stress is always compressive, and is much higher than that for applied tension. Hence the interface is able to sustain much higher shear stresses in compression than for tension where extensive slipping

and tensile separation occurs thereby restricting the shear stresses at the interface .

The rate of load transfer for a given applied load ($p/\sigma_0=\pm5$) as a function of μ is shown in Fig. 9 ($p>0$, tensile) and Fig. 10 ($p<0$, compressive). As expected, the load diffusion is much faster for higher coefficients of friction, and in compression, it approaches that for the perfectly bonded interface for sufficiently high μ (Fig. 10). The load diffusion in the fiber under the constant shear stress approximation is shown in the form of broken lines in Figs. 9 and 10. The development length, L_d, required in this case to diffuse the fiber load completely is given by [4]

$$L_d/a = |p|/\tau_0, \tag{12}$$

where $\tau_0 = \mu\sigma_0$ is the constant shear stress at the interface.

The constant interface shear strength approximation neglects differences between tensile and compressive loads on the fiber. It is observed that for compressive loadings, the diffusion rate is faster than that for the constant shear stress approximation, while it is slower for applied tension. Unlike the constant shear stress approximation, which gives a discrete cutoff load dissipation length, L_d, it is seen that for a frictional restraint, a small residual stress is retained in the fiber and decreases exponentially with depth.

Slip at the surface.

Tensile (or compressive) loads applied on the fiber causes an extraction (or indentation) given by the slip between the fiber and matrix at the surface. The slip at the surface Δ_s, normalized by $ap(\kappa + 1)/G$ (where $\kappa = 3-4\nu$ for plane strain, G is the shear modulus of the fiber material) is plotted as a function of the normalized load $p/\mu\sigma_0$ in Fig. 11. The results are similar to those presented in Dollar et. al. [4], though our results indicate that for compression, slip at the surface is somewhat greater than that in [4]. For the constant interface shear strength approximation Δ_s is given by [4]

$$\Delta_s G/\{ap(\kappa+1)\} = p/(16\mu\sigma_0), \tag{13}$$

and is plotted in the form of broken lines in Fig. 11.

SUMMARY AND CONCLUSIONS

Preliminary results obtained from the finite element model of the pullout test show good agreement with analytical solutions predicted by Dollar et. al. [4]. Further investigation is necessary to obtain appropriate values for E_{nn} and E_{tt} for inhomogeneous interfaces, and to study stress distributions for a system of proximate fibers embedded in the matrix in contrast to the case of an isolated fiber. It is seen that interfacial stress characteristics for a frictionally restrained interface is different from that obtained from the simple constant shear stress approximation, at least for the case of an isolated fiber. It is not presently known however whether such frictional modeling would affect the overall strength characteristics of composites significantly, and whether such a degree of sophistication is justified. The interface friction elements may be easily incorporated into existing micromechanical analytic models for brittle matrix composites (such as the local-global model developed by Ballarini et, al. [7]), which presently assume a constant shear strength at the fiber-matrix interface. They could also be used to study problems involving complicated and finite geometries, and to analyze size effects on interface behavior. This would make model assumptions very realistic, and render them amenable for the analysis of a wide range of composites. Such constitutive local-global modeling using the interface friction elements is presently under investigation and will be reported in a future communication.

ACKNOWLEDGEMENTS

This work was supported by the NASA-Lewis Research Center, under Grant no. NAG3-856.

REFERENCES

1. Aveston, J., Cooper G. A., Kelley A., "Single and Multiple Fracture", The Properties of Fibre Composites, IPC Science and Technology Press, Guildford, England, pp. 15-26. 26, 1971.

2. Budiansky, B., Hutchinson J. W., and Evans A. G., "Matrix fracture in fiber-reinforced ceramics", Journal of the Mechanics and Physics of Solids, Vol. 34, No. 2, pp. 167-189, 1986.

3. Marshall, D. B., Cox B. N., Evans A. G., "Mechanics of matrix cracking in brittle-matrix fiber composites", Acta Metallurgica, Vol. 33, No. 11, pp. 2013-2021, 1985.

4. Dollar A. and Steif P. S., "Load transfer in composites with a coulomb friction interface", International Journal of Solids and Structures, Vol. 24, No. 8, pp. 789-803, 1988.

5. Ballarini, R., Parulekar A., and Plesha, M. E., "Finite Element Modeling of Discontinuities with Dilatancy and Surface Degradation", Engineering Fracture Mechanics, in press.

6. Plesha, M. E., "Constitutive Models for Rock Discontinuities with Dilatancy and Surface Degradation", International Journal of Numerical and Analytic Methods in Geomechanics, Vol. 11, pp. 345-362, 1987.

7. Ballarini, R., and Ahmed S., "Local-Global Analysis of Crack Growth in Continuously Reinforced Ceramic Matrix Composites", NASA CR-182231, NASA Lewis Research Center, Cleveland, OH, 1988.

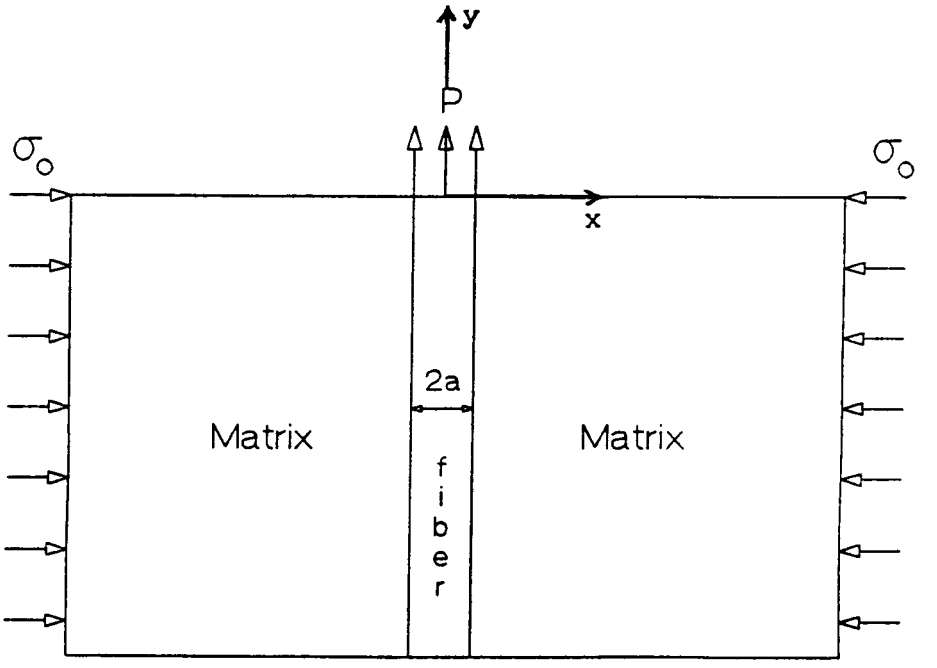

Fig. 1. Setup for the fiber pullout test.

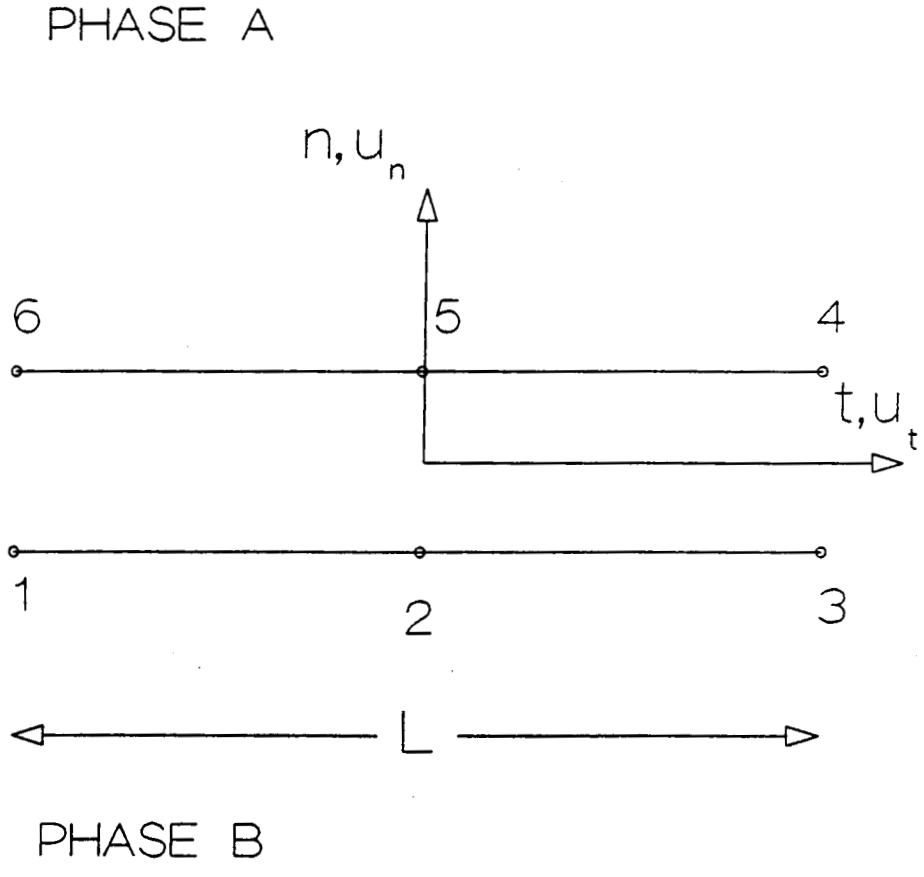

Fig. 2. The interface friction element.

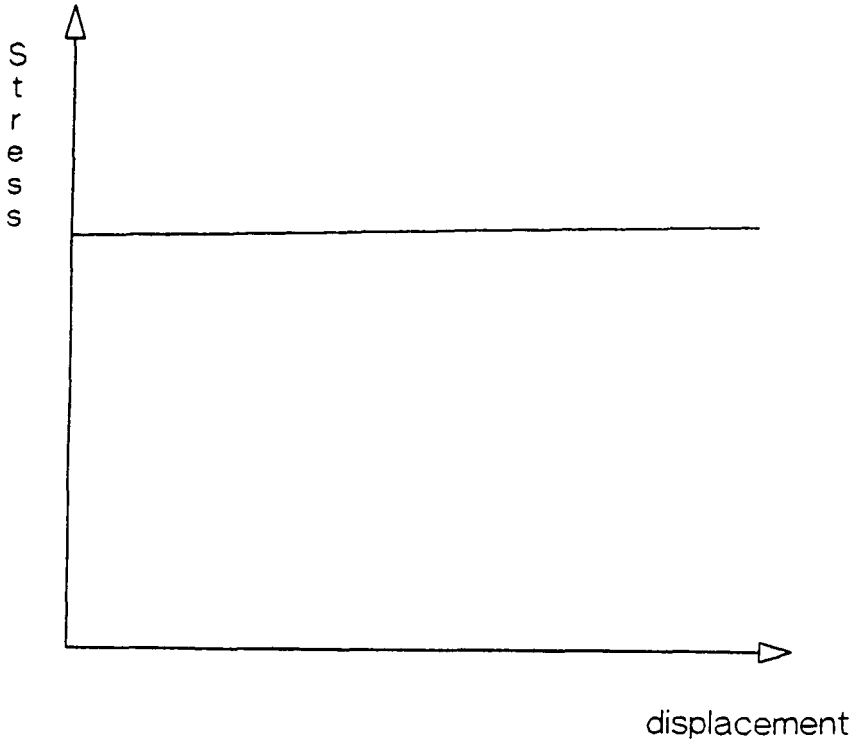

Fig. 3. The rigid-perfectly plastic response required of the interface element.

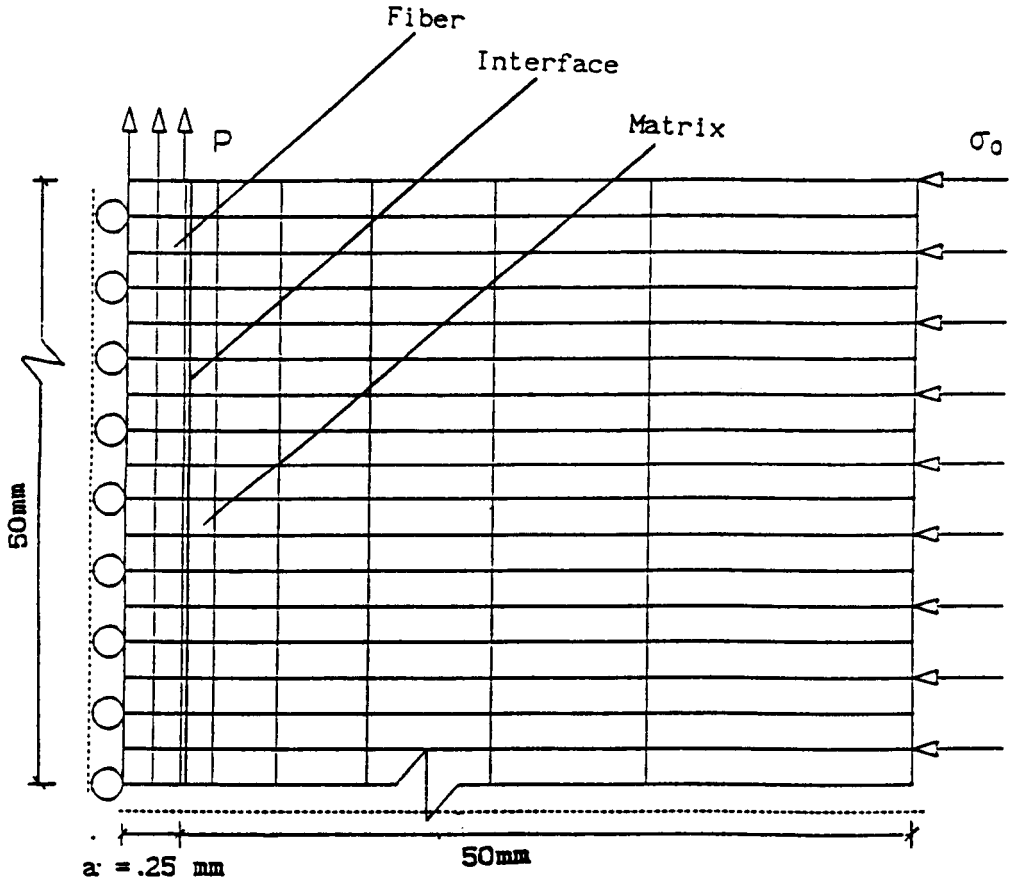

Fig. 4. Finite element mesh for the fiber pullout test. (not to scale)

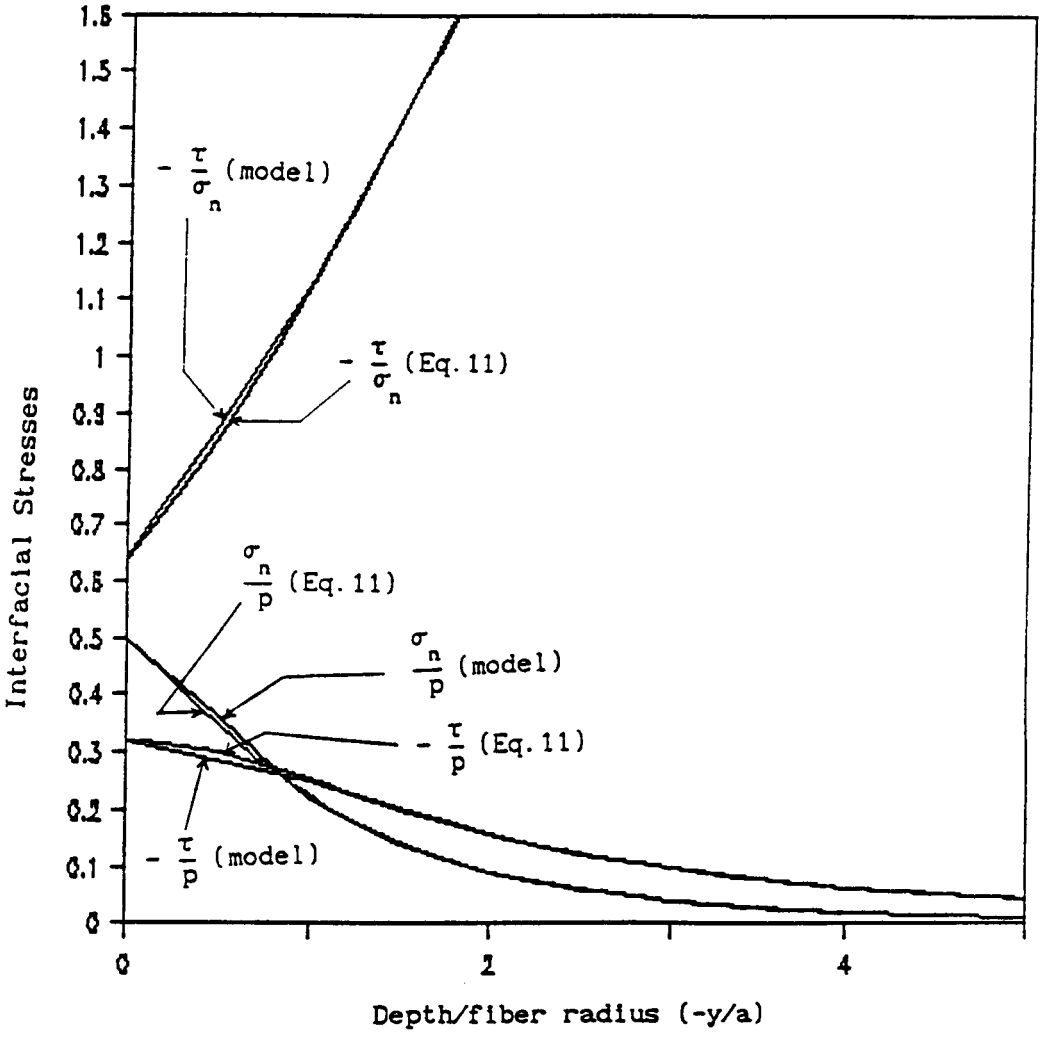

Fig. 5. Distribution of normal (σ_n) and tangential (τ) interfacial stresses for a perfectly bonded interface

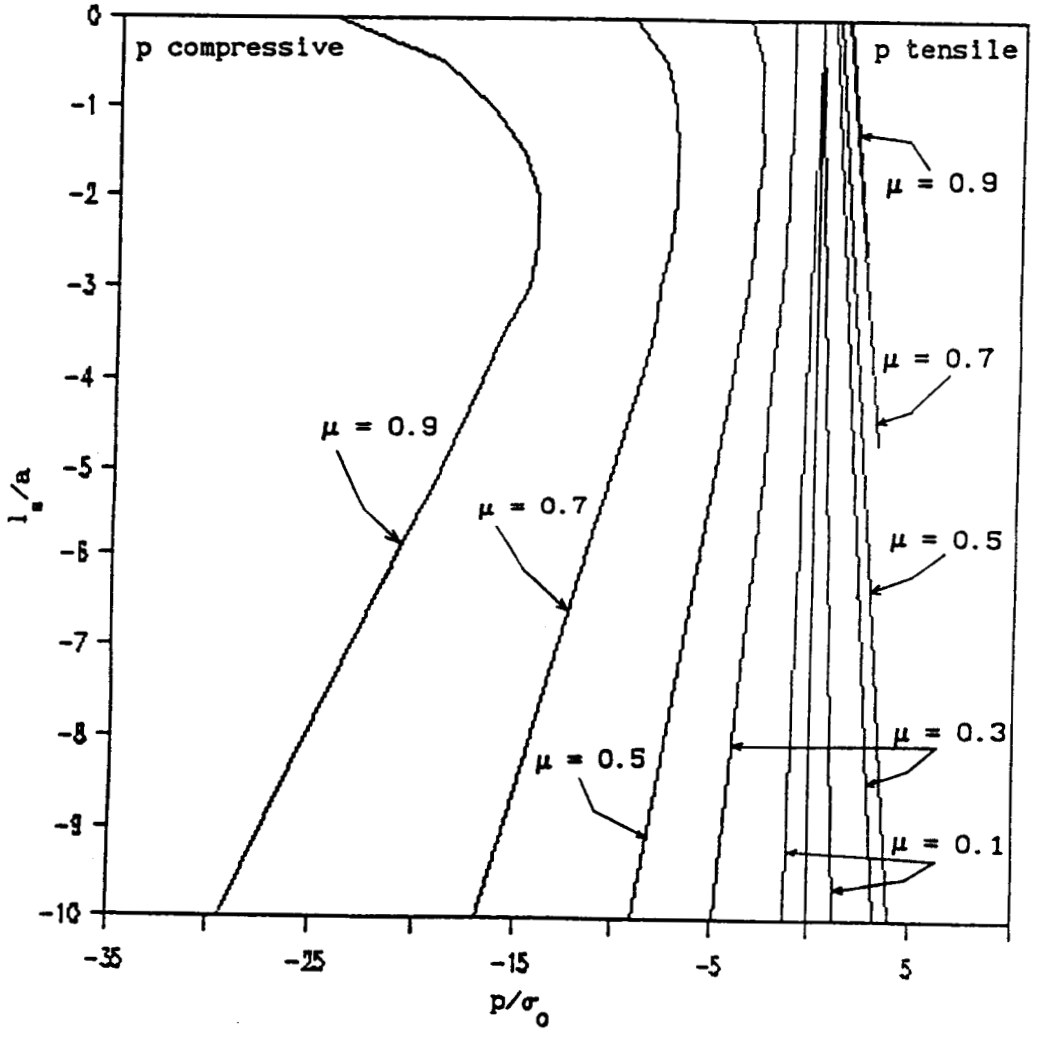

Fig. 6. Extent of slip as a function of the normalized load p/σ_0.

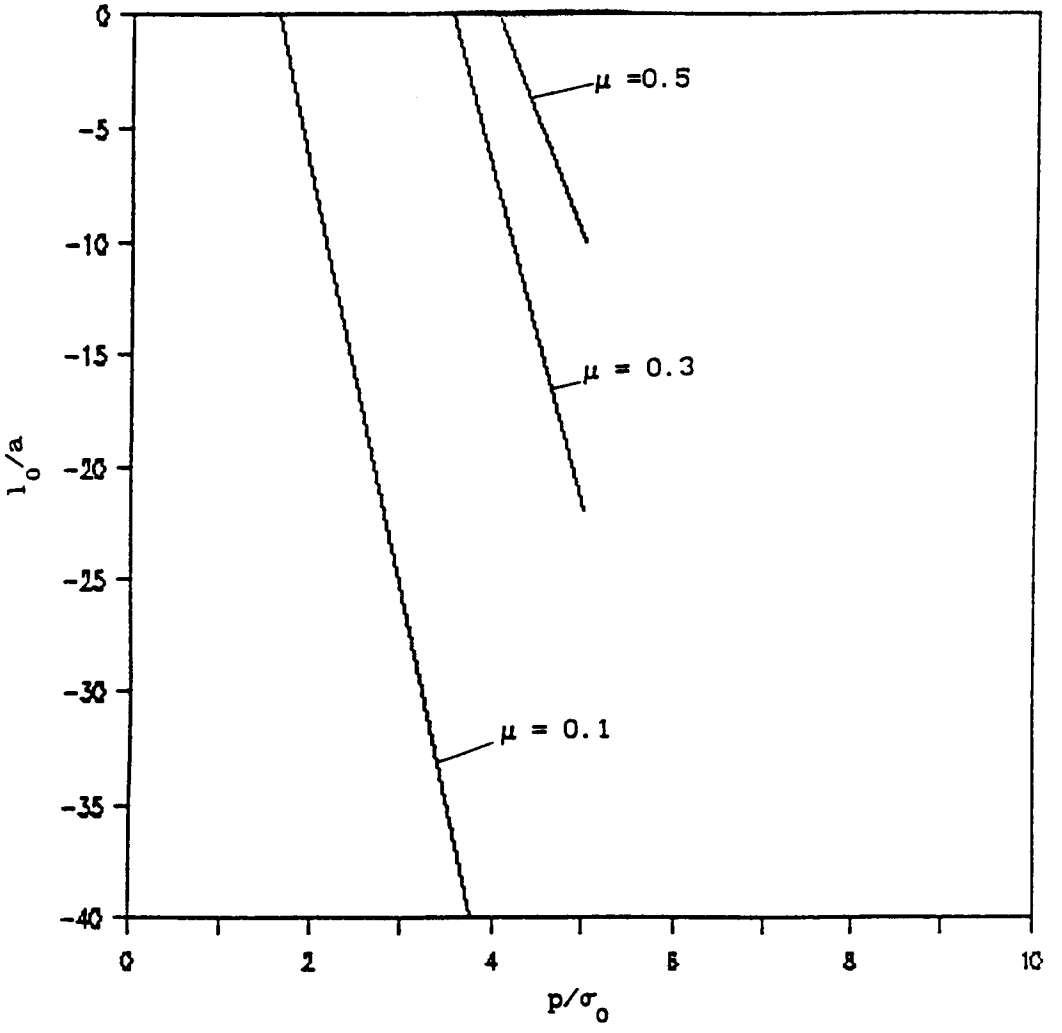

Fig. 7. Extent of delamination l_0 as a function of the normalized tensile load p/σ_0

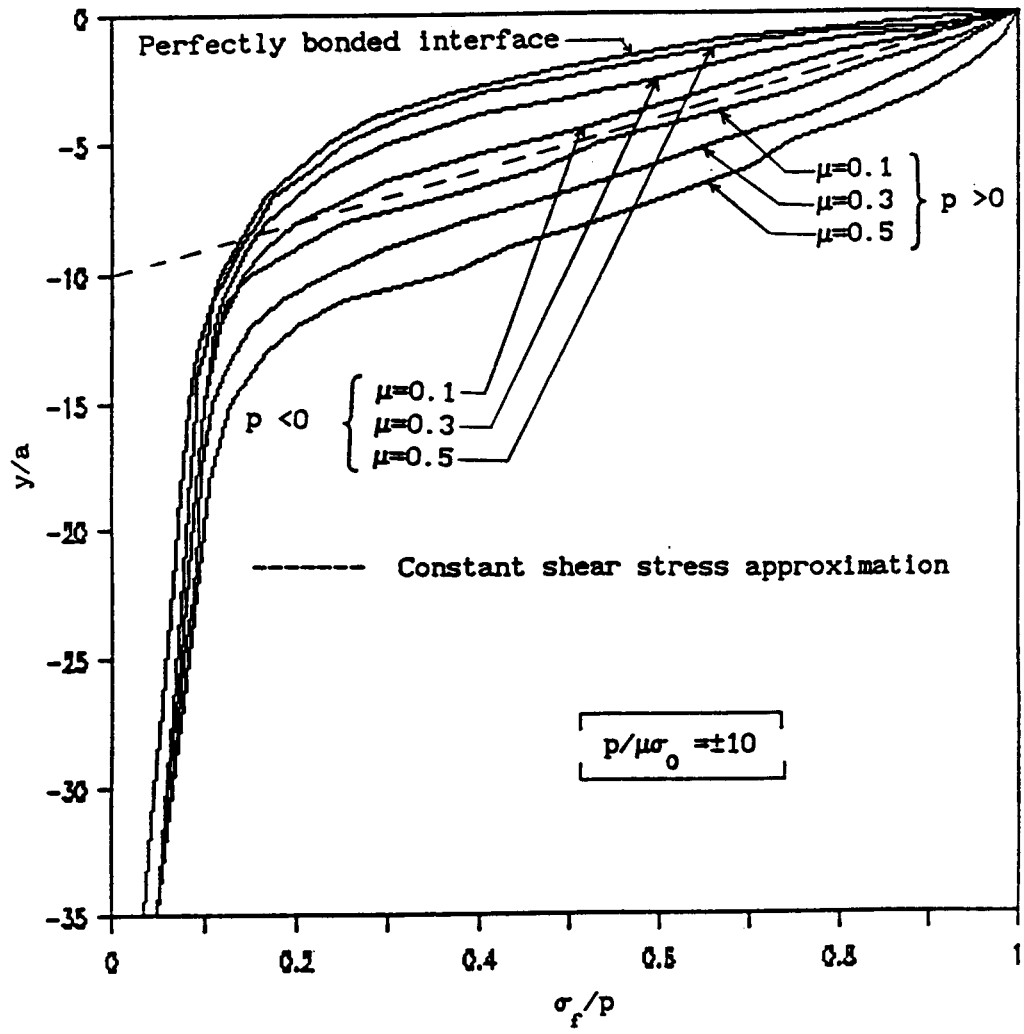

Fig. 8. Load diffusion from fiber to matrix for tensile and compressive loadings ($p/\mu\sigma_0 = \pm 10$)

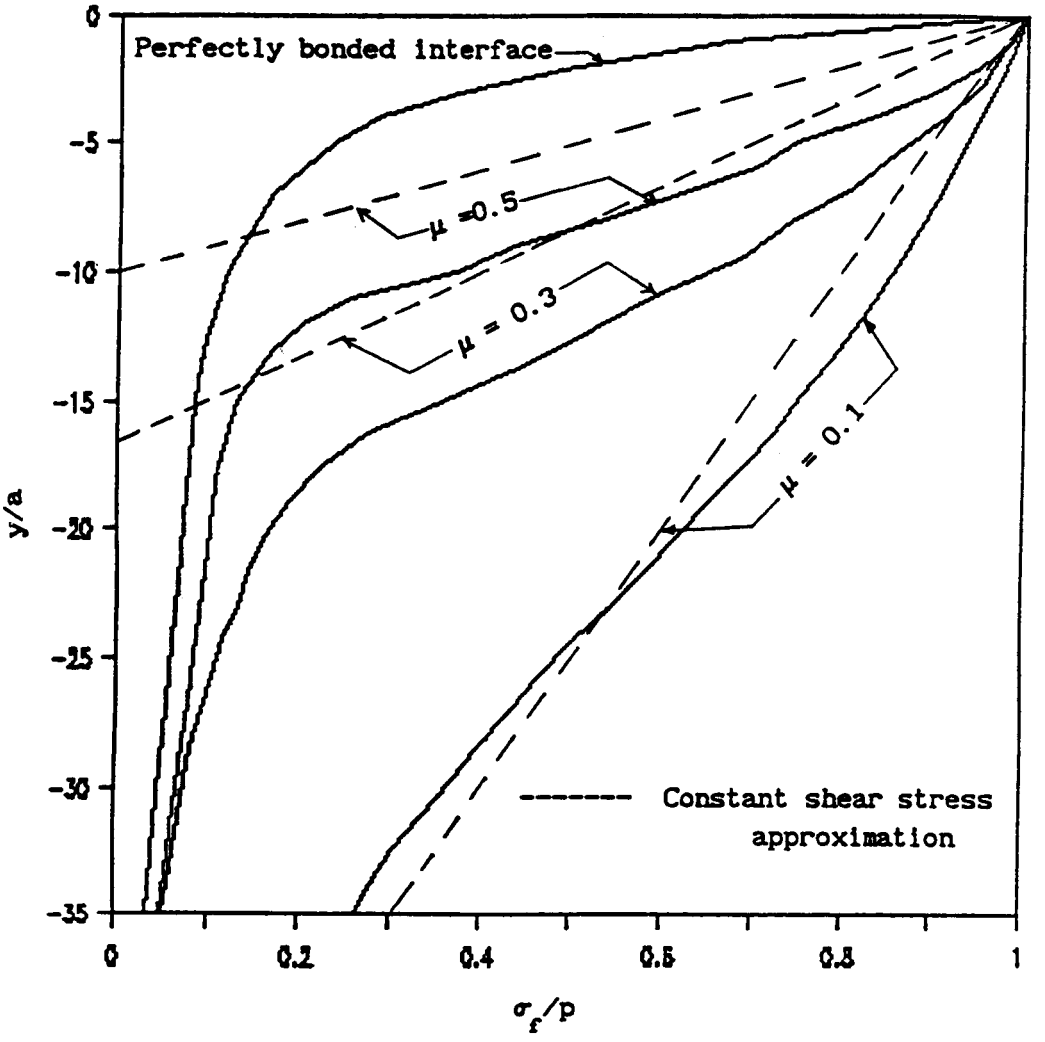

Fig. 9. Fiber load diffusion for tensile loading ($p/\sigma_0 = 5$)

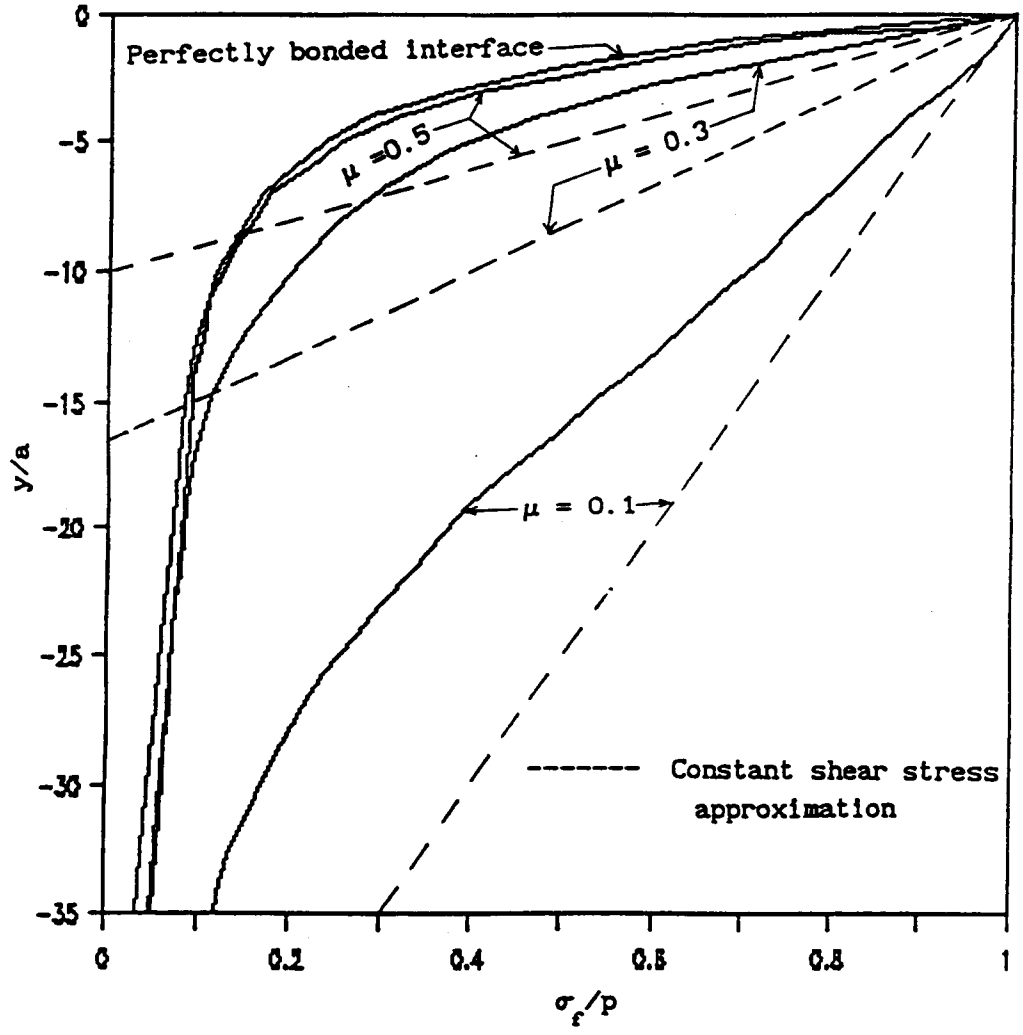

Fig. 10. Fiber load diffusion for compressive loading ($p/\sigma_0 = -5.0$).

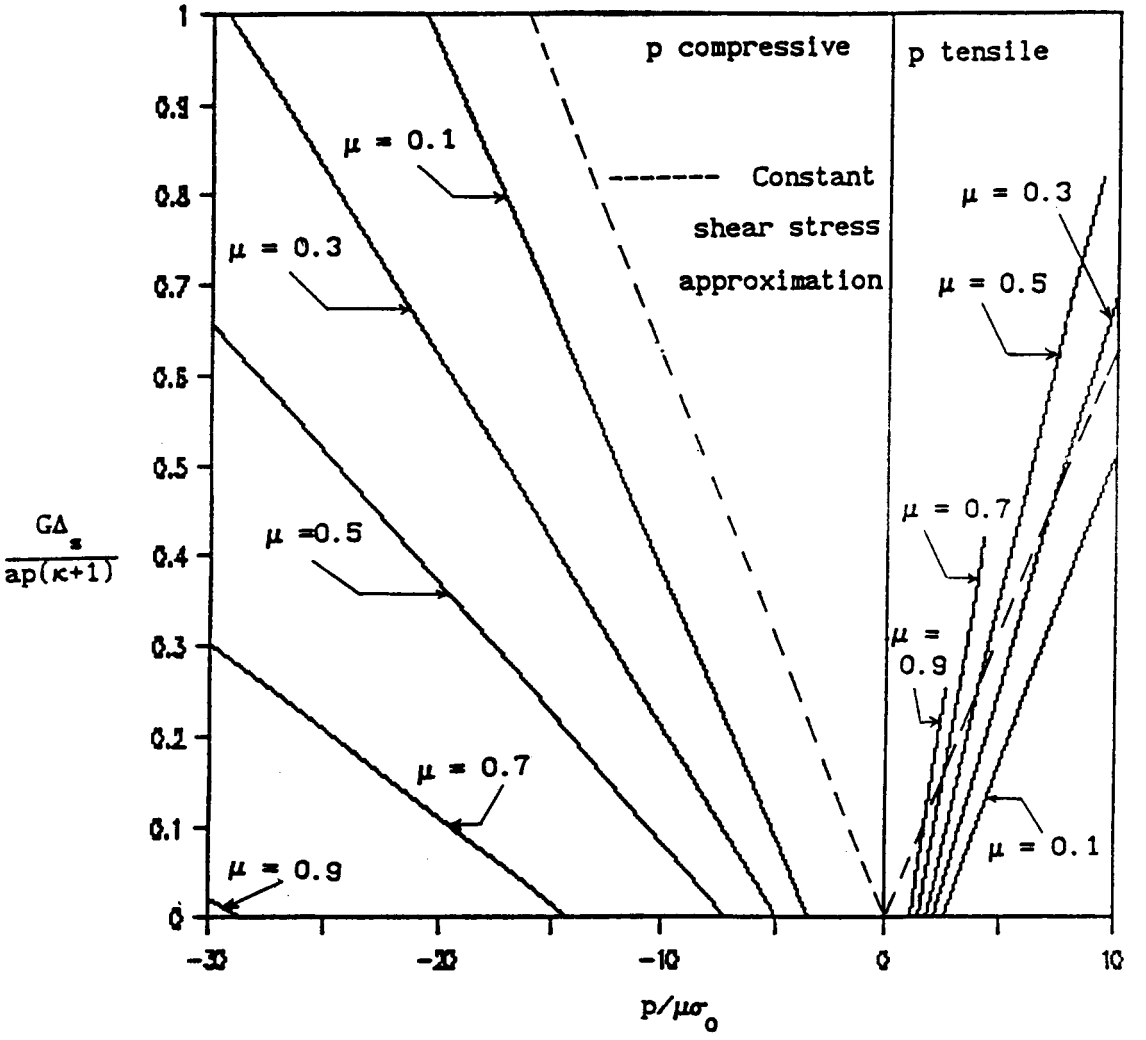

Fig. 11. Slip at the surface for tensile and compressive loadings as a function of the renormalized load $p/\mu\sigma_0$.

NASA
National Aeronautics and Space Administration

Report Documentation Page

1. Report No.	2. Government Accession No.	3. Recipient's Catalog No.
NASA CR-182281		

4. Title and Subtitle	5. Report Date
Finite Element Modeling of Frictionally Restrained Composite Interfaces	April 1989
	6. Performing Organization Code

7. Author(s)	8. Performing Organization Report No.
Roberto Ballarini and Shamim Ahmed	None
	10. Work Unit No. 505-63-31

9. Performing Organization Name and Address	11. Contract or Grant No.
Case Western Reserve University Department of Civil Engineering Cleveland, Ohio 44106	NAG3-856
	13. Type of Report and Period Covered Contractor Report Final
12. Sponsoring Agency Name and Address	14. Sponsoring Agency Code
National Aeronautics and Space Administration Lewis Research Center Cleveland, Ohio 44135-3191	

15. Supplementary Notes

Project Manager, Bernard Gross, Structures Division, NASA Lewis Research Center.

16. Abstract

This paper describes the use of special interface finite elements to model frictional restraint in composite interfaces. These elements simulate Coulomb friction at the interface, and are incorporated into a standard finite element analysis of a two-dimensional isolated fiber pullout test. Various interfacial characteristics, such as the distribution of stresses at the interface, the extent of slip and delamination, load diffusion from fiber to matrix, and the amount of fiber extraction or depression are studied for different friction coefficients. The results are compared to those obtained analytically using a singular integral equal approach [4], and those obtained by assuming a constant interface shear strength. The usefulness of these elements in micromechanical modeling of fiber-reinforced composite materials is highlighted.

17. Key Words (Suggested by Author(s))	18. Distribution Statement
Composite interface Special interface finite element Fiber pullout	Unclassified – Unlimited Subject Category 39

19. Security Classif. (of this report)	20. Security Classif. (of this page)	21. No of pages	22. Price*
Unclassified	Unclassified	23	A03

*For sale by the National Technical Information Service, Springfield, Virginia 22161